

See discussions, stats, and author profiles for this publication at: <https://www.researchgate.net/publication/255818870>

Filamentation and temporal reshaping of a femtosecond pulse in fused silica

Article in *Physical Review A* · December 2003

DOI: 10.1103/PhysRevA.68.063820

CITATIONS

47

READS

19

5 authors, including:



Zhaoxin Wu

Xi'an Jiaotong University

115 PUBLICATIONS 991 CITATIONS

SEE PROFILE



Quan Sun

Hokkaido University

36 PUBLICATIONS 466 CITATIONS

SEE PROFILE



Yang Hong

Sensata Technologies Inc.

45 PUBLICATIONS 339 CITATIONS

SEE PROFILE

All content following this page was uploaded by [Quan Sun](#) on 18 February 2016.

The user has requested enhancement of the downloaded file. All in-text references [underlined in blue](#) are added to the original document and are linked to publications on ResearchGate, letting you access and read them immediately.

Filamentation and temporal reshaping of a femtosecond pulse in fused silica

Zhaoxin Wu, Hongbing Jiang,* Quan Sun, Hong Yang, and Qihuang Gong†

Department of Physics & State Key Laboratory for Mesoscopic Physics, Peking University, Beijing 100871, People's Republic of China

(Received 9 May 2003; published 23 December 2003)

The filamentation of a focused femtosecond pulse in fused silica was systemically investigated both experimentally and numerically. We observed the different filamentation of a laser pulse under different external focusing conditions and input energy experimentally. For instance, a focused femtosecond laser pulse with an energy of $3.3 \mu\text{J}$ induced a long electron plasma filament for an effective numerical aperture (NA) of 0.01 of focusing objective, an electron plasma filament with two-foci structure for 0.04 effective NA, and a short filament for effective NA of 0.09. In theory, the numerical results of the extended nonlinear Schrödinger (NLS) equation agreed with experimental results under different focusing conditions and energy. Moreover, under different focusing conditions we found the filamentation is connected with different temporal reshaping behaviors, and the temporal compression of the reshaped laser pulse in propagation is responsible for the two-foci structure of an electron plasma filament.

DOI: 10.1103/PhysRevA.68.063820

PACS number(s): 42.65.Jx, 42.65.Sf, 42.25.Bs, 42.65.Re

I. INTRODUCTION

Filamentation and propagation of a laser pulse is one of the most fundamental nonlinear optical processes, and the recent development of sources of intense femtosecond laser pulses has added many interesting twists to this long-standing problem. For instance, the laser pulse with 100 fs duration and intensities limited to 10^{13} W/cm^2 form the long-range filament in the atmosphere [1–5]. This phenomenon results from the dynamical competition between the self-focusing (SF) and defocusing of electron plasma. For input powers that are above the critical power P_{cr} for SF, the laser beam focuses over a finite distance and undergoes catastrophic collapse according to the steady-state theory of SF. In fact, the on-axis beam intensity increases through this process until multiphoton ionization occurs [6]. The induced electron plasma defocuses the beam and arrests the catastrophic collapse of the beam by SF. At powers around critical, the balance between SF and defocusing of electron plasma can result in the long-range filament.

In conjunction with the research on filamentation of a femtosecond laser pulse in air, the propagation of a femtosecond laser pulse in transparent solid, such as fused silica, glass, and sapphire, was studied [7–9]. This propagation is more complex than that in air. Besides the defocusing of electron plasma, other processes can also arrest the catastrophic collapse of a laser beam by SF. For instance, the combined effect of SF and normal group velocity dispersion (GVD) leads to pulse splitting, which limits the collapse of the laser pulse [8,10,11]. In the literature [7], under soft focusing condition a long self-guide light channel was observed as a single laser pulse was focused into fused silica by a lens of 8-mm focal length, and a corresponding long filament induced by a light channel was attributed to the same mechanism as that in air, that is, the dynamic balance between multiple photon ionization (MPI) and SF. In our pre-

vious study [12], however, the filamentation of a focused ultrashort laser pulse in fused silica was found to be quite different under the different focusing condition. Under a tight focusing condition, using a higher numerical aperture (NA) objective, the investigation of nonlinear propagation and filamentation of focused ultrashort laser pulses is a more important subject because it is widely used in the application of the bulk transparent material processing and micromachining [13,14]. However, the dynamic of propagation and filamentation of an ultrashort laser pulse in transparent solid media has not been studied systematically under different focusing conditions.

In this paper, the nonlinear propagation and filamentation of a focused ultrashort laser pulse under different focusing conditions in fused silica were investigated both experimentally and numerically. We observed that a filament induced by an ultrashort laser pulse takes on a long filament when the effective NA of the focusing objective is 0.01. In the case of the focusing objective with effective NA 0.04 and an input pulse energy of $3.3 \mu\text{J}$, the induced plasma filament exhibits the two-foci structure, and for the focusing objective with effective NA 0.09, the induced plasma filament shows a short filament. Results of numerical simulation for the extended nonlinear Schrödinger (NLS) equation involving the self-focusing effect, temporal dispersion, impact ionization, and MPI are found to be in good agreement with experimental results. The numerical results suggest the clear dynamic processes of nonlinear propagation of a focused ultrashort laser pulse under different focusing conditions in fused silica, and reveal the temporal reshaping of the pulse under different focusing conditions. They show that the ultrashort laser pulse temporal reshaping is closely connected with filamentation. As for an induced plasma filament with two-foci structure, the second focus in the filament directly results from the temporal compression of the reshaped pulse.

II. EXPERIMENT SETUP AND RESULTS

A Ti:sapphire chirped pulse amplification laser with a pulse duration of 120 fs and a wavelength at 800 nm was

*Email address: hbjiang@pku.edu.cn

†Email address: qhgong@pku.edu.cn

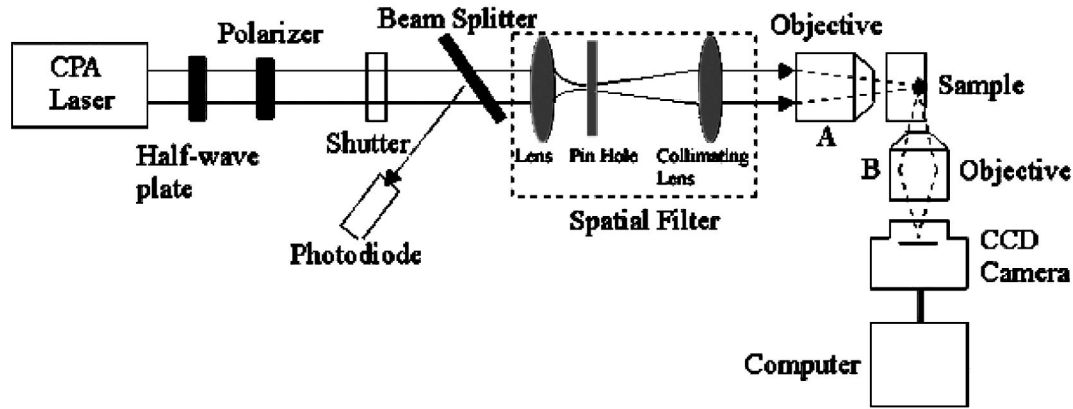


FIG. 1. Experiment setup.

used in our experiment. The repetition rate of the laser is 10 Hz. Figure 1 gives the schematic of the experimental setup. The interaction of a single pulse with the fused silica was studied and the single laser pulse was chosen by an electronic shutter during the exposal time of the CCD camera. A spatial filter was employed to obtain the high beam quality. The objective ($4\times$) with NA of 0.15 was chosen to focus the laser beam. The energy of the input laser pulse was monitored by a calibrated photodiode. The laser beam was collimated by the lens after the pinhole with focal lengths of 20 cm, 40 cm, and 100 cm, which obtained the different focusing condition. Plasma luminescence was imaged on a CCD camera by objective *B*. By adjusting the compressor grating separation to compensate the temporal chirp induced by a polarizer, lenses, and focusing objective, the pulse duration was minimized to be 300 fs at the focal region of the objective lens *A*.

In the experiment, we use the effective NA to describe the geometric focusing effect of the objective. For a given objective, its effective NA will vary with the radius of the collimated laser beam in the input aperture of the objective. When the lenses with focal length $f=20$ cm, $f=40$ cm, and $f=100$ cm were used to collimate the laser beam, the waist of the laser beam at the focal region was measured to be $14.6\ \mu\text{m}$, $6.1\ \mu\text{m}$, and $2.8\ \mu\text{m}$, respectively. The corresponding effective NA of objective *A* was calculated to be 0.01, 0.04, and 0.09, respectively.

Figures 2(a)–2(c) show the images of plasma luminescence induced by the ultrashort laser pulse using focusing objectives with an effective NA of 0.01, 0.04, and 0.09, respectively. The input energy of the pulse is $2.1\ \mu\text{J}$. The laser beam was incident from left to right. Figure 2(a) shows a long electron plasma filament and Figs. 2(b) and 2(c) show the short filaments and the corresponding on-axis relative intensities of plasma luminescence. When the energy of the laser pulse is increased to $3.3\ \mu\text{J}$, the corresponding plasma filaments are shown in Figs. 3(a), 3(b), and 3(c). In Figs. 3(a), 3(b), and 3(c), the corresponding on-axis relative intensities of plasma luminescence were also presented. For the case of 0.01 effective NA, Fig. 3(a) show a longer plasma filament; for the case of 0.04 effective NA, Fig. 3(b) shows a

filament with two-foci structure; and for the case of 0.09 effective NA, the filament takes on one peak structure in Fig. 3(c). Figure 4 shows the damaged track for the case of Fig. 3(b), which was observed by an optical microscope (Olympus IX70).

III. NUMERICAL RESULTS AND DISCUSSIONS

In order to analyze and understand the mechanism of non-linear propagation of a focused ultrashort laser pulse in fused

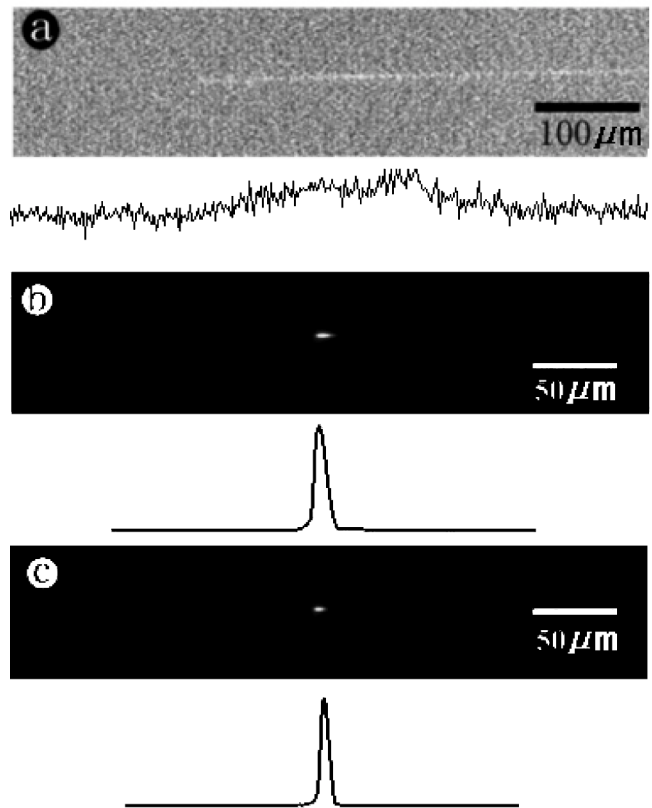


FIG. 2. Photomicrographs and the on-axis relative intensities of plasma luminescence. The energy of the pulse is $2.1\ \mu\text{J}$. The effective NA of the objective is (a) 0.01, (b) 0.04, and (c) 0.09. The laser pulse is incident from left to right.

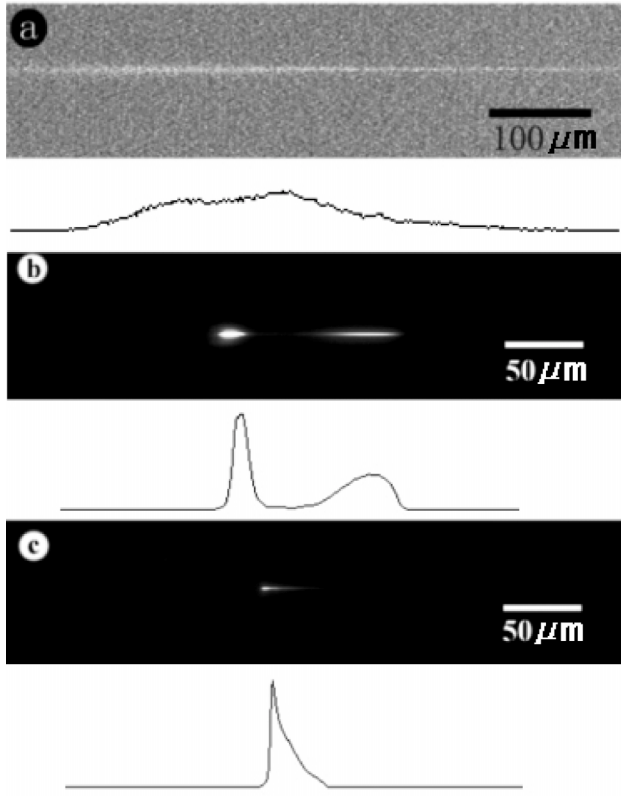


FIG. 3. Photomicrographs and the on-axis relative intensities of plasma luminescence. The energy of the pulse is $3.3 \mu\text{J}$. The effective NA of the objective is (a) 0.01, (b) 0.04, and (c) 0.09.

silica, we start with a physical model, which was developed for the intense pulse propagation in fused silica [7,12], gas [15], air [16], and water [17],

$$\left(i2k \frac{\partial}{\partial z} + \nabla_{\perp}^2 \right) E = kk'' \frac{\partial^2 E}{\partial \xi^2} - ik\sigma(1 + i\omega\tau)\rho E - ik\beta^K |E|^{2K-2} E - 2kk_0 n_2 |E|^2 E, \quad (1)$$

$$\frac{\partial \rho}{\partial \xi} = \frac{1}{n^2} \frac{\sigma}{E_g} \rho |E|^2 + \frac{\beta^{(K)} |E|^{2K}}{K\hbar\omega} - \frac{\rho}{\tau_r}. \quad (2)$$

Equation (1) is the (3D+1)-dimensional NLS equation including GVD, absorption, and defocusing by the plasma, multiphoton absorption (MPA), and the effect of SF. Equation (2) is a coupled equation which comes from the Drude model, considering avalanche ionization, MPI, and electron

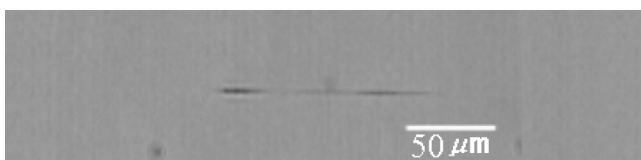


FIG. 4. Photograph of the damaged track viewed by an optical microscope under the same condition as Fig. 3(b).

recombination. $E(r, z, \xi)$ is the electric-field envelope expressed in the retarded coordinate system, $\xi = t - z/v_g$, v_g is the group velocity, ω and $|E|^2$ are the frequency and intensity of a laser, $k = n\omega/c$, $k'' = \partial^2 k / \partial \omega^2 = 360 \text{ fs}^2/\text{cm}$ in fused silica [18], ρ is the electron density, σ is the cross section for inverse bremsstrahlung, and $\sigma = (ke^2\tau') / \{ \omega m_e \epsilon_0 [1 + (\omega\tau')^2] \} = 2.78 \times 10^{-18} \text{ cm}^2$ [7,16]. $\beta^{(6)} = 6.1 \times 10^{-63} \text{ cm}^{11} \text{ W}^{-6}$ is the K -photon absorption coefficient [19]. The band-gap energy of fused silica is $E_g = 9.0 \text{ eV}$ [14], yielding a number of photons $K = 6$. The critical power for SF is $P_{\text{cr}} = 0.159\lambda_0^2 / nn_2$ [16], $n = 1.46$, and $n_2 = 2.5 \times 10^{-16} \text{ cm}^2/\text{W}$ [18]. The characteristic time $\tau_r = 150 \text{ fs}$ in fused silica is used to describe the electron recombination [20]. Equations (1) and (2) are assumed to be cylindrical symmetry.

Equation (1) was solved by the alternating direction implicit method (ADI), which is a general finite-difference method to solve the multiple dimensional partial difference equation numerically and is recognized as conditionless stable. The initial conditions for numerical simulation are from our experiment. The pulse duration is 300 fs, and initial pulse energies are $3.3 \mu\text{J}$ and $2.1 \mu\text{J}$, corresponding to powers $P_{\text{in}} = 3.1 P_{\text{cr}}$ and $2.0 P_{\text{cr}}$. It is assumed that the initial laser pulse keeps Gaussian shape in space and time, so the initial electric field envelope has the form

$$E(0, r, \xi) = \sqrt{\frac{2P_{\text{in}}}{\pi a^2(0)}} \exp\left(-\frac{r^2}{a^2(0)} - \frac{\xi^2}{\tau_0^2} - \frac{ikr^2}{2f} \right),$$

where $a(0)$ is the initial radius of the laser beam. Here we chose the radius of laser beam at the entrance surface of the sample as $a(0)$. f is the distance between the entrance surface of the sample and the focus of the laser beam in the fused silica. NA can be expressed by $a(0)/\sqrt{f^2 + a(0)^2}$.

Figures 5, 6, 7, 8, 9, and 10 show the numerical results by solving Eqs. (1) and (2) numerically. Figures 5(a)–5(c) show the 3D electron plasma filaments and the profile of on-axis electron density of the filaments for the input pulse energy of $2.1 \mu\text{J}$ ($P_{\text{in}} = 2.0 P_{\text{cr}}$) under the same focusing conditions as those in Figs. 2(a)–2(c). Figure 5(a) shows the long electron plasma filament and Figs. 5(b) and 5(c) show the short filament, which agrees well with the experimental results in Figs. 2(a)–2(c). Figures 6(a)–6(c) show the 3D electron plasma filaments and the profile of on-axis electron density of filaments for the input pulse energy of $3.3 \mu\text{J}$ ($P_{\text{in}} = 3.1 P_{\text{cr}}$) under various focusing conditions as Fig. 3. Figure 6(a) show a long plasma channel for the case of 0.01 effective NA. For the case of 0.04 effective NA, the electron plasma filament takes on a two-peak structure, shown in Fig. 6(b). Figure 6(c) gives the numerical simulation of an electron plasma filament for the 0.09 effective NA. These numerical results agree well with the experimental results, shown in Fig. 3.

For the case of 0.01 effective NA and $P_{\text{in}} = 3.1 P_{\text{cr}}$, Fig. 7(a) shows the on-axis maximum intensity along propagation direction corresponding to Fig. 6(a). For the input power P_{in} that is above the critical power P_{cr} of self-focusing, steady-state theory predicts that the pulse will undergo catastrophic

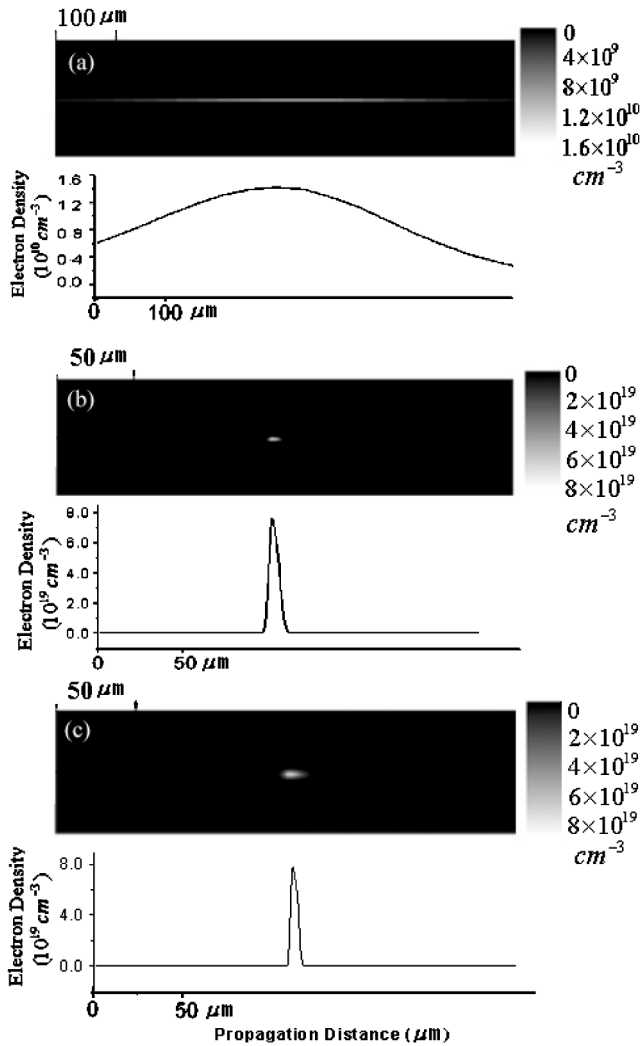


FIG. 5. Numerical results of 3D and on-axis distribution of electron plasma density induced by an ultrashort laser pulse in propagation. The input pulse power is $P_{in}=2.0 P_{cr}$ and pulse energy is $2.1 \mu\text{J}$. The effective NA is (a) 0.01, (b) 0.04, and (c) 0.09, respectively.

collapse [21]. When the effective NA is small, the laser pulse propagates a long distance before reaching the focus of the laser beam. The self-focusing and GVD play a significant role in propagation. The catastrophic collapse of the laser pulse will be arrested by the temporal splitting of the pulse, which results from the combined effect of self-focusing and GVD [8,10,11]. Figure 7(b) (solid line) shows the temporal splitting pulse at the position of $z=800 \mu\text{m}$. The temporal splitting leads to the change of on-axis intensity and induced electron plasma density, which are shown in Figs. 7(a) and 6(a). The split pulse was temporally compressed by the effect of self-focusing [20], reached a much higher intensity at the position $z=1200 \mu\text{m}$, and then decayed, as shown in Fig. 7(a). Figure 7(c) shows the temporal profile of the pulse at a different position in propagation.

When the effective NA of the objective is 0.04 and $P_{in}=3.1 P_{cr}$, Fig. 8(a) shows on-axis maximum intensity along propagation direction corresponding to Fig. 6(b). The large

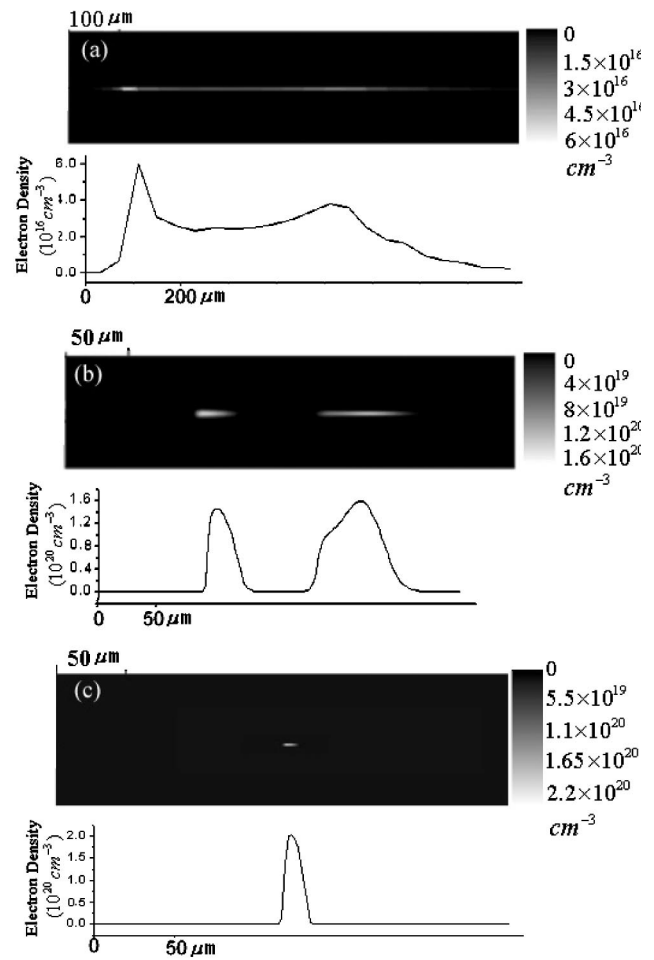


FIG. 6. Numerical results of 3D and on-axis distribution of electron plasma density induced by an ultrashort laser pulse in propagation. The effective NA is (a) 0.01, (b) 0.04, and (c) 0.09, respectively. The input pulse power $P_{in}=3.1 P_{cr}$ and the energy of the pulse is $3.3 \mu\text{J}$.

effective NA of the objective means that the laser pulse propagates a short distance before reaching the focus. The high intensity near the focus can ionize fused silica and leads to a prompt increase of electron plasma density. MPI and absorption of the induced electron plasma by MPI and avalanche ionization, instead of the pulse-splitting by SF and GVD, stop the catastrophic collapse of the laser beam by SF, and limit the increase of intensity of the laser pulse by self-focusing and geometric focusing. The electron plasma generated by the leading edge of the pulse defocuses the remainder of the pulse because of the negative refractive index of plasma. This would lead to the decrease of on-axis laser intensity and electron plasma density. As a result, the first focus of the laser beam is formed in propagation, shown in Figs. 8(a) and 6(b). The solid, dotted, and dashed profiles in Fig. 8(b) show that the pulse was shortened by the defocusing of the trail edge of the pulse. Figure 8(b) (dotted-dashed line) shows that the pulse exhibits a two-pulse profile temporally. The leading peak, occurring at earlier time, is directly associated with the single peak in Fig. 8(b) (solid, dotted, dashed line), and the trailing peak develops out of the

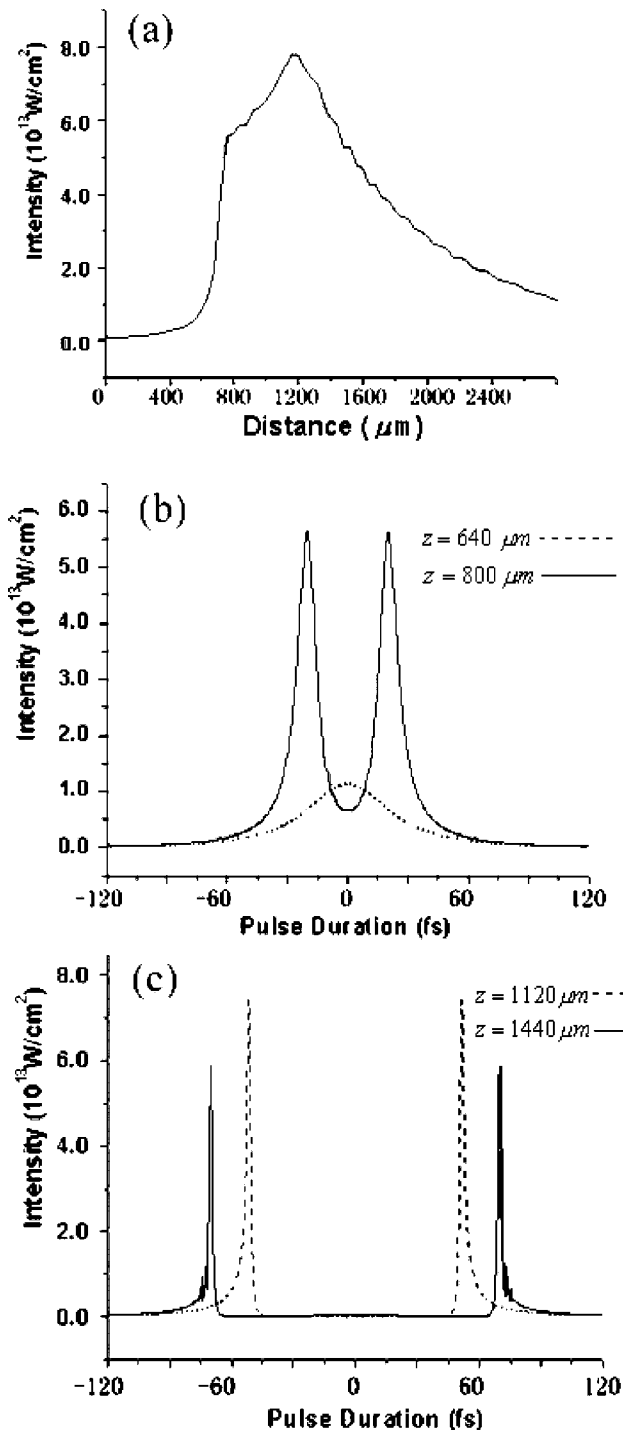


FIG. 7. (a) On-axis maximum intensity as functions of propagation distance corresponding to Fig. 6(a). Temporal profiles of the pulse at position of (b) $z = 640 \mu\text{m}$ (dotted line), $800 \mu\text{m}$ (solid line) and (c) $z = 1120 \mu\text{m}$ (dotted line), $1440 \mu\text{m}$ (solid line). The energy of the pulse is $3.3 \mu\text{J}$. The effective NA of the objective is 0.01.

background. Owing to the decrease of on-axis electron density, the defocused trailing edge of the pulse in the spatial domain refocuses again by SF, which results in the formation of the trailing peak in the temporal domain. The leading pulse in the temporal domain decays owing to multiple pho-

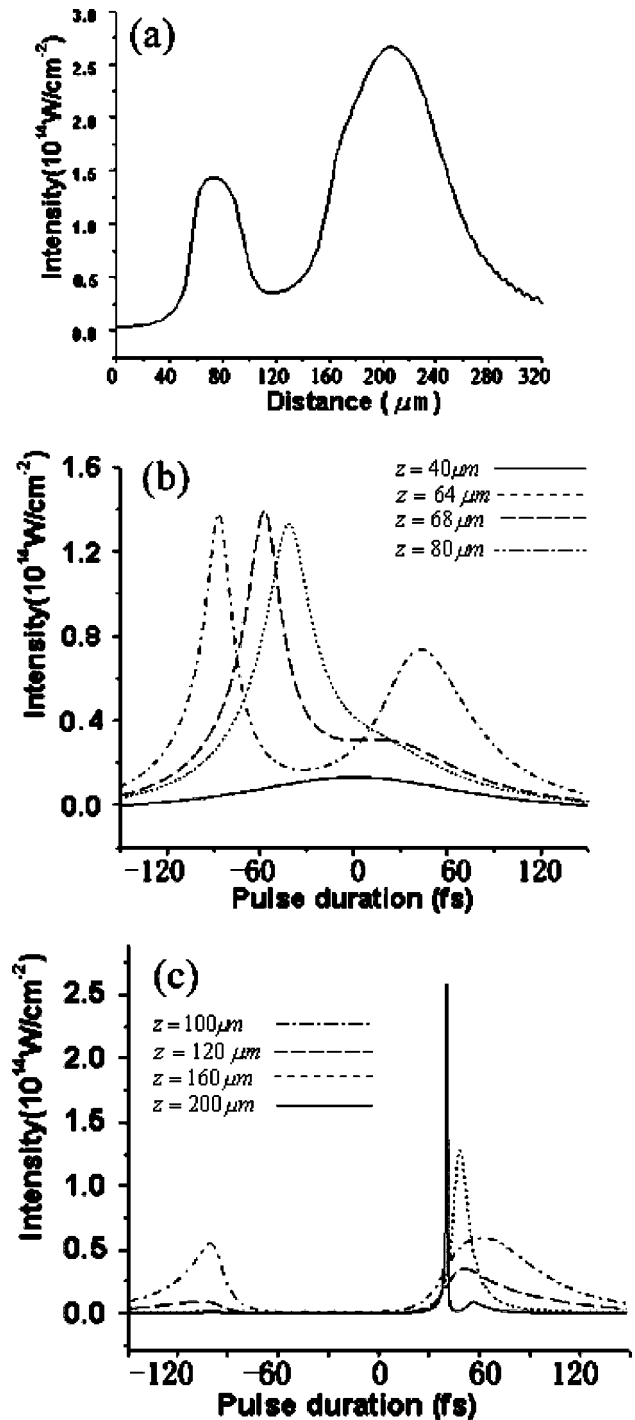


FIG. 8. (a) On-axis maximum intensity as functions of propagation distance corresponding to Fig. 6(b). Temporal profiles of the pulse at position of (b) $z = 40 \mu\text{m}$ (solid line), $64 \mu\text{m}$ (dotted line), $68 \mu\text{m}$ (dashed line), $68 \mu\text{m}$ (dashed line), $80 \mu\text{m}$ (dotted and dashed line) and (c) $z = 120 \mu\text{m}$ (dashed line), $160 \mu\text{m}$ (dotted line), $200 \mu\text{m}$ (solid line). The energy of the pulse is $3.3 \mu\text{J}$. The effective NA of the objective is 0.04.

ton absorption (MPA) and absorption by plasma, but the trailing pulse in the temporal domain continuously increases and refocuses because the defocused trailing edge of the pulse is converged by self-focusing, shown in Fig. 8(c) (dot-

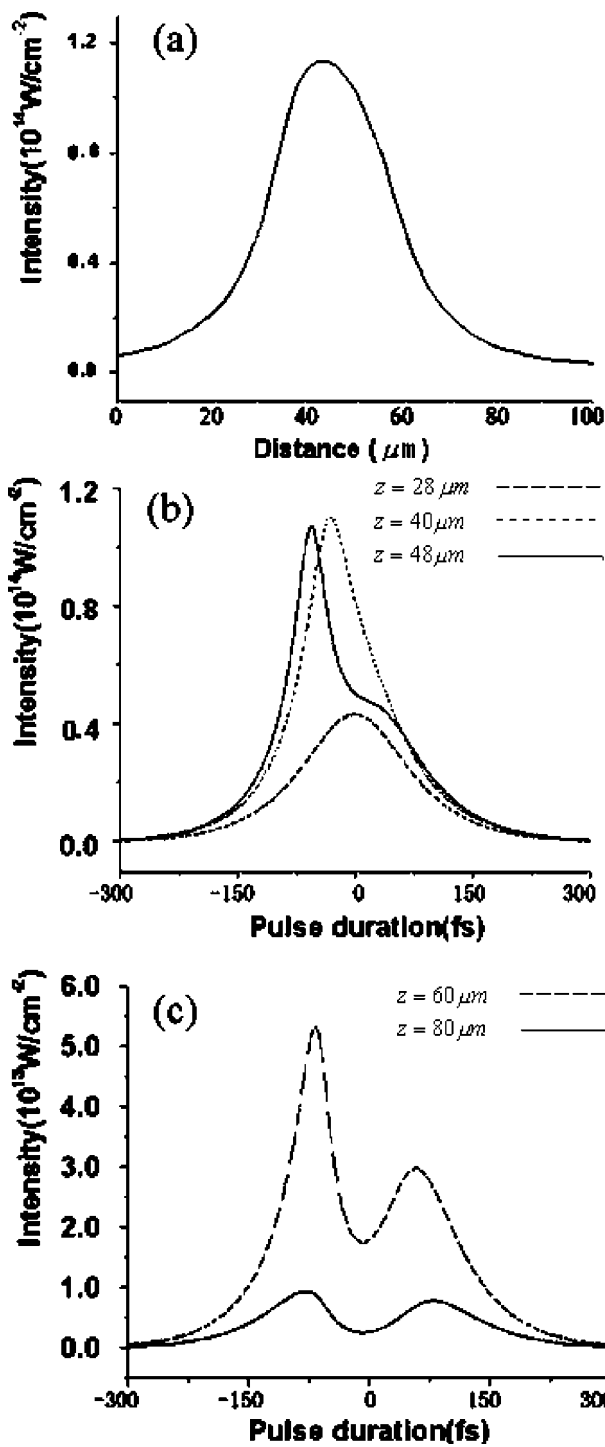


FIG. 9. (a) On-axis maximum intensity as functions of propagation distance corresponding to Fig. 5(b). Temporal profiles of the pulse at position of (b) $z = 28 \mu\text{m}$ (dashed line), $40 \mu\text{m}$ (dotted line), $48 \mu\text{m}$ (solid line), and (c) $z = 60 \mu\text{m}$ (dashed line), $80 \mu\text{m}$ (solid line). The energy of the pulse is $2.1 \mu\text{J}$. The effective NA of the objective is 0.04.

ted line and dashed line). This dynamic process is similar to the model of “dynamic spatial replenishment,” which was used to describe the nonlinear propagation of a femtosecond laser pulse in air [16]. Moreover, the trailing pulse was temporally compressed to a few femtoseconds by self-focusing

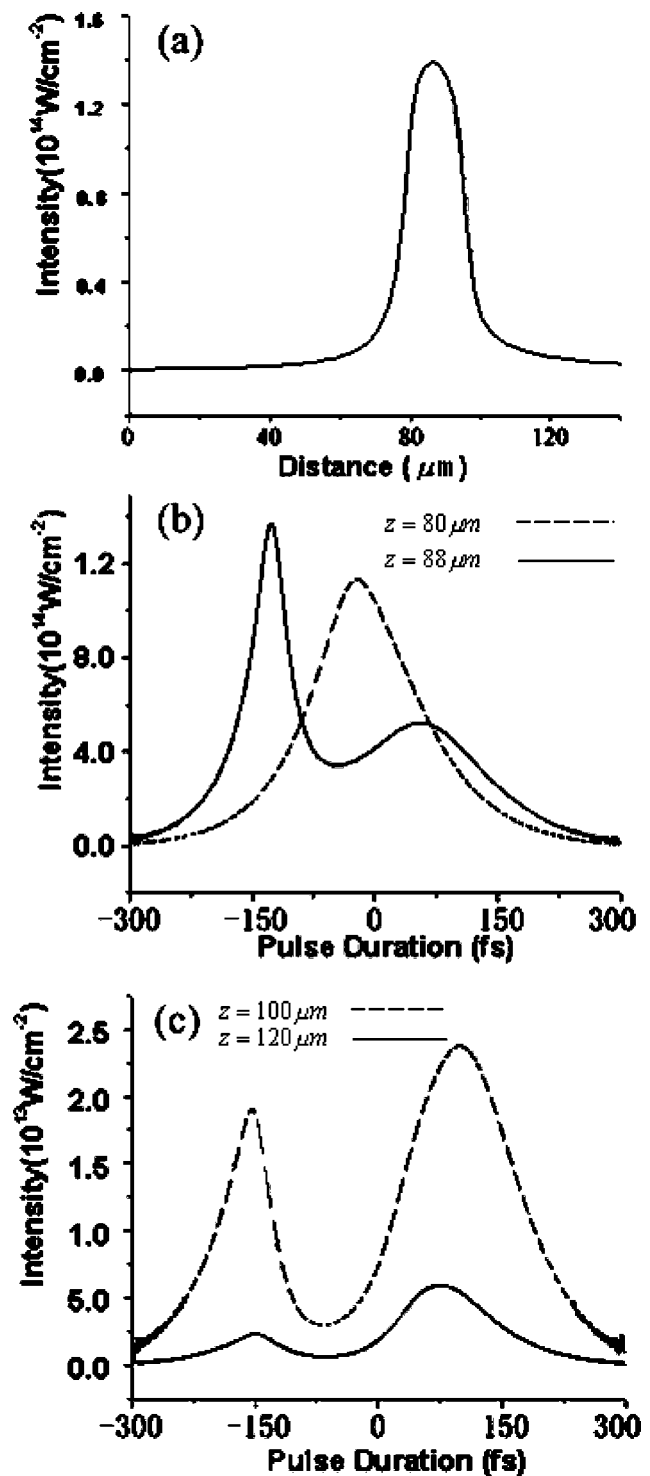


FIG. 10. (a) On-axis maximum intensity as functions of propagation distance corresponding to Fig. 6(c). Temporal profiles of the pulse at position of (b) $z = 80 \mu\text{m}$ (dashed line), $88 \mu\text{m}$ (solid line) and (c) $z = 100 \mu\text{m}$ (dashed line), $120 \mu\text{m}$ (solid line). The energy of the pulse is $3.3 \mu\text{J}$. The effective NA of the objective is 0.09.

and MPI [20,22–24], shown in Fig. 8(c) (solid line). The shortened trailing pulse reaches higher intensity, which leads to the second peak in the plasma filament at last, shown in Fig. 6(b), and this is the reason why the two-peak structure occurs in the nonlinear propagation and filamentation in Fig.

8(a). For a lower input power, $P_{\text{in}}=2.0 P_{\text{cr}}$, Fig. 9(a) shows the on-axis maximum intensity along the propagation direction corresponding to Fig. 5(b), which is quite different from the case of $P_{\text{in}}=3.1 P_{\text{cr}}$. The lower power of the pulse generates less electron plasma, and not enough energy of the pulse is defocused spatially by the electron plasma. Then the trailing pulse is temporally formed with lower intensity and the pulse duration cannot be compressed by SF and MPI for its lower intensity, which are shown in Figs. 9(b) and 9(c). So only one focus in propagation is formed, shown in Figs. 5(b) and 9(a).

Both Figs. 7(b) (solid line) and 8(b) (dotted-dashed line) show the double-pulse profile, but they are different. The former results from the interaction between SF and normal GVD, and the two pulses develop simultaneously. The latter comes from interaction between SF and the defocusing of electron plasma for the trailing edge of the pulse, and the leading pulse develops first, followed by the trailing pulse. These show the different dynamic processes of nonlinear propagation for effective NA 0.01 and 0.04, and lead to the different filamentation, shown in Figs. 6(a), 6(b), 7(a), and 8(a).

As for the higher effective NA of objective 0.09 and $P_{\text{in}}=3.1 P_{\text{cr}}$, Fig. 10(a) shows on-axis maximum intensity along the propagation direction corresponding to Fig. 6(c). The dynamic process of nonlinear propagation is quite similar to that in the case of 0.04 effective NA. At the position of $z=88 \mu\text{m}$, the double-pulse profile is formed by the same mechanism as that in the case of 0.04 effective NA, shown in Fig. 10(b) (solid line). However, as the shorter Rayleigh length of the laser beam for 0.09 effective NA, the intensity of the trailing pulse is attenuated spatially by diffraction and the compression of the trailing pulse is avoided, shown in Fig. 10(c). Thus, only one peak, instead of a two-peak structure, was formed in the nonlinear propagation and filamentation, shown in Figs. 6(c) and 10(a).

In comparison with the nonlinear propagation of a focused laser pulse under 0.01, 0.04, and 0.09 effective NA, input pulse energy $P_{\text{in}}=3.1 P_{\text{cr}}$, we found temporal reshaping of the pulse presents different behaviors and is associated with filamentation in propagation. For 0.01 effective NA, the pulse was split by the combined effect of SF and normal GVD and a long electron filament was formed in propagation. For 0.04 effective NA of the objective, the input pulse was temporally reshaped into a two-pulse profile by the defocusing of induced plasma and SF. The leading pulse decayed and the trailing pulse was temporally compressed to a few femtoseconds and reached a higher intensity and led to the two-foci structure in nonlinear propagation and filamentation. For 0.09 effective NA, the dynamic process of pulse propagation is the same as that for 0.04 effective NA, except that the trailing pulse cannot be compressed because of a shorter Rayleigh length of the laser beam, and this formed one focus of the laser pulse in propagation, unlike the case of 0.04 effective NA. For the case of $P_{\text{in}}=2.0 P_{\text{cr}}$ and 0.04 effective NA, the input pulse was also reshaped into a two-pulse profile temporally, but the trailing pulse cannot be

compressed sharply because of low energy, which shows one peak in filamentation. The compression of the trailing pulse in the temporal reshaping of the pulse is responsible for the two-foci structure of nonlinear propagation and filamentation.

The temporal compression of an ultrashort laser pulse in transparent ionizing media was also observed by other groups [22–24]. In the above analysis of dynamic processes of the nonlinear propagation of a femtosecond laser pulse, we presented the dependence of the temporal compression of a pulse on the focusing parameter and energy of a laser beam, shown in Figs. 7, 8, 9, and 10. As the potential application in pulse shortening techniques, our numerical results on temporal compression of an ultrashort laser pulse in transparent ionizing media could present the optimum conditions in the applications.

In addition, by comparing the damaged zone by the filament in Fig. 4 with the numerical result in Fig. 6(b), we find the electron density generated by MPI and avalanche ionization in the damaged zone is close to 10^{20} cm^{-3} , which is the same as the theoretical results in Sudrie *et al.* [25].

IV. CONCLUSION

In conclusion, in experiment we systemically investigated the filamentation of a focused femtosecond laser pulse by objective with various effective NA and input pulse energy in fused silica. The two foci structure of a plasma filament and the damaged zone in fused silica were observed and studied. In theory, we studied the nonlinear propagation and filamentation of a femtosecond laser pulse in fused silica by solving the NLS equation numerically. Our numerical results of plasma filaments agreed well with the experimental results, and our numerical analysis presented the clear dynamic processes of nonlinear propagation of a focused femtosecond laser pulse by objective with different effective NA and pulse energy in fused silica. It was found that the pulse was temporally reshaped in nonlinear propagation, and under different focusing conditions and input energy the behaviors of pulse temporal reshaping were quite different. In the case of effective NA 0.04 and $P_{\text{in}}=3.1 P_{\text{cr}}$, the pulse was reshaped and can be compressed to a few femtoseconds. Moreover, our numerical analysis revealed that the filamentation is connected with the temporal reshaping of the pulse in nonlinear propagation, and the compression of trailing pulse leads to the two foci structure of nonlinear propagation and plasma filament.

ACKNOWLEDGMENTS

The work was supported by the National Key Basic Research Special Foundation (NKBRFSF) under Grant No. G1999075207, and the National Natural Science Foundation of China under Grant Nos. 90101027, 10104003, and 90206003. The project was also supported by Youth Teacher's Foundations of National Education Committee and the Scientific Research Foundation for Returned Overseas Chinese Scholars of National Education Committee.

- [1] A. Braun *et al.*, *Opt. Lett.* **20**, 73 (1995).
- [2] E. T. J. Nibbering *et al.*, *Opt. Lett.* **21**, 62 (1996).
- [3] A. Brodeur *et al.*, *Opt. Lett.* **22**, 304 (1997).
- [4] L. Wöste *et al.*, *Laser Optoelektron.* **29**, 51 (1997).
- [5] H. R. Lange *et al.*, *Opt. Lett.* **23**, 120 (1998).
- [6] L. V. Keldysh, *Sov. Phys. JETP* **20**, 1307 (1965).
- [7] S. Tzortzakis *et al.*, *Phys. Rev. Lett.* **87**, 3902 (2001).
- [8] J. K. Ranka, R. W. Schirmer, and A. L. Gaeta, *Phys. Rev. Lett.* **77**, 3783 (1996).
- [9] A. L. Gaeta, *Phys. Rev. Lett.* **84**, 3582 (2000).
- [10] P. Chernev and V. Petrov, *Opt. Lett.* **17**, 172 (1992).
- [11] J. E. Rothenberg, *Opt. Lett.* **17**, 583 (1992).
- [12] Z. Wu *et al.*, *Opt. Lett.* **27**, 448 (2002).
- [13] Y. Li *et al.*, *Opt. Lett.* **26**, 1912 (2001).
- [14] C. B. Schaffer *et al.*, *Opt. Lett.* **26**, 93 (2001).
- [15] M. D. Feit and J. A. Fleck, *Appl. Phys. Lett.* **24**, 169 (1974).
- [16] M. Mlejnek, E. M. Wright, and J. V. Moloney *Opt. Lett.* **23**, 382 (1998).
- [17] Q. Feng *et al.*, *IEEE J. Quantum Electron.* **33**, 127 (1997).
- [18] A. A. Zozulya *et al.*, *Phys. Rev. Lett.* **82**, 1430 (1999).
- [19] M. Lenzner *et al.*, *Phys. Rev. Lett.* **18**, 4076 (1998).
- [20] P. Audebert *et al.*, *Phys. Rev. Lett.* **73**, 1990 (1994).
- [21] J. H. Marburger and W. G. Wanger, *IEEE J. Quantum Electron.* **3**, 415 (1967); G. L. McAllister, J. H. Marburger, and L. G. DeShazer, *Phys. Rev. Lett.* **21**, 1648 (1968).
- [22] [Hélène Ward and Luc Bergé, *Phys. Rev. Lett.* **90**, 053901 \(2003\).](#)
- [23] I. G. Kppinkov *et al.*, *Phys. Rev. Lett.* **84**, 2000 (2000).
- [24] M. Nurhuda *et al.*, *Phys. Rev. A* **66**, 023811 (2002).
- [25] L. Sudrie *et al.*, *Phys. Rev. Lett.* **89**, 6601 (2002).